

Effect of melt treatment, solidification conditions and porosity level on the tensile properties of 319.2 endchill aluminium castings

A.M. SAMUEL, F.H. SAMUEL

Département des Sciences Appliquées, Université du Québec à Chicoutimi, 555 Boulevard de l'Université, Chicoutimi (Québec) G7H 2B1 Canada

An experimental investigation of the tensile properties of endchill castings of 319.2 commercial aluminium alloy was carried out to determine the effect of Sr modifier, TiB₂ grain refiner and hydrogen content, and the resulting porosity on these properties. It was found that with respect to solidification time, the interaction effect of other parameters on the porosity followed the order H₂ > Sr > TiB₂. Pore nucleation and pore morphology were solidification time-dependent, with Sr addition enhancing the sphericity of the pores. Both ultimate tensile strength (UTS) and ductility were sensitive to variations in porosity and solidification conditions, while the yield strength remained practically unaffected. Increase in the porosity volume fraction above 0.5% reduced the ductility to negligible levels in the unmodified, non-grain refined base alloy. It was also observed that Sr modification and grain refining allow for an increase in the porosity level before the same level of degradation in ductility is reached.

1. Introduction

Among cast aluminium alloys, 319 ranks as one of the commercially important alloys used in automotive applications, on account of its excellent casting characteristics and good mechanical properties. Today, with the increasingly critical nature of component specifications, likewise demands are posed on the strength, ductility, and quality of these components, necessitating a close monitoring of the various alloy and process parameters involved. Obviously, the most important of these is the solidification or cooling rate which, in addition to its effect on the microstructure, also affects the amount of porosity. Porosity is the other important factor, determined mainly by the hydrogen level of the alloy melt, as well as by its "cleanliness" in terms of inclusions and oxide films present therein. Both factors are responsible, to a major extent, for the resultant properties.

Controlling the microstructure can also be done through grain refinement and modification, where small additions of Al–Ti–B and Al–Sr master alloys, respectively, provide the necessary impetus for the production of refined microstructures and the required morphology of constituent phases.

The correlation of microstructure (through the dendrite arm spacing (DAS)) with mechanical properties in directionally solidified castings of A356 alloy have been reported by several investigators [1–3]. Their results indicate that the ultimate tensile strength (UTS) is inversely proportional to the DAS, the elongation has a parabolic relation to the DAS, while the yield strength (YS) is practically not affected by the

solidification conditions. These observations may be generalized for most casting alloys, provided the castings obtained are sufficiently sound.

The relationship between porosity and any of the mechanical properties is non-linear [4]. The shape of the non-linear graphs obtained gives an indication of the pronounced influence of porosity on the properties, specially at lower porosity levels, where even an increase of about 0.5% in porosity can bring down the strength and ductility to dangerously low levels. Among the properties measured, UTS appears to be the one most affected by porosity, followed by YS and percentage elongation. In their study of the effect of solidification parameters on the feeding efficiency of A356 alloy, Pan *et al.* [5] have shown that the UTS-percent porosity relationship is linear, whereas the percentage elongation-percent porosity relation is a logarithmic one.

Compared to A356 alloy, relatively little is to be found in the literature on similar studies regarding the performance of 319 alloy. The present work forms part of an ongoing research programme aimed at investigating the effect of solidification parameters and porosity content on the tensile properties of 319 aluminium automotive alloy.

2. Experimental procedure

The 319.2 aluminium alloy used in this study was supplied in the form of 12.5-kg ingots. The chemical composition of the as-received alloy is shown in Table I. The ingots were melted in a silicon carbide

TABLE I Chemical composition of the as-received 319.2 alloy (wt %)

Si	Cu	Fe	Mn	Mg	Ti	Zn	Ni	Sr
6.23	3.77	0.46	0.14	0.06	0.073	0.08	0.008	0.0003

crucible of 7 kg capacity, using an electrical resistance furnace. The melting temperature was held at $735 \pm 5^\circ\text{C}$. At this temperature the molten metal was either degassed using high purity argon (melt hydrogen content $\sim 0.1 \text{ ml } 100 \text{ g}^{-1}$ Al—designated H1) or gassed (melt hydrogen content $0.22\text{--}0.24 \text{ ml } 100 \text{ g}^{-1}$ Al—designated H2; or $\sim 0.32\text{--}0.36 \text{ ml } 100 \text{ g}^{-1}$ Al—designated H3). Melts were also modified with strontium (with Sr levels of $\sim 70\text{--}90$ p.p.m—designated S1; $120\text{--}180$ p.p.m—designated S2; $250\text{--}310$ p.p.m—designated S3) in the form of Al–10 wt % Sr master alloy, and grain refined by means of Al–5 wt % Ti–1 wt % B master alloy, to obtain a 0.02 wt % Ti content (designated T).

The AlScan™ unit is one of the commercial techniques available to provide direct measurements of the hydrogen content in the melt. The melt temperature is measured simultaneously. In the present work, the melt hydrogen level was monitored using an AlScan™ unit. In addition, specimens were also cast simultaneously in Ransley moulds (for each pouring/casting) from which “Ransley” samples were machined for determination of hydrogen content using the Leco vacuum fusion technique. This is one of the standard methods for obtaining accurate analysis of the hydrogen content in a melt. For each pouring, specimens for chemical analysis were also taken.

It has been reported that direct readings of the hydrogen content in liquid metal with AlScan™ exceed the hydrogen content measured from Ransley samples using the Leco subfusion technique [6]. In the present work, this was found to be so, except in those cases where Sr was added to the melt, in which case the AlScan™ and Leco readings differed greatly and showed an opposite trend. Table II shows a comparison between AlScan and Leco readings at different levels of Sr and hydrogen. It is evident that in the presence of Sr, the AlScan readings are considerably lower than those obtained from the Leco method ($\Delta H_2 = [(AlScan - Leco) / AlScan]\%$). This difference, however, did not exist when the AlScan readings were taken *before* the addition of Sr. The exact explanation of this phenomenon is beyond the scope of the present study.

Casting was done in a rectangular shape endchilled mould, with dimensions $64 \times 127 \times 254 \text{ mm}$, as shown in Fig. 1 [6]. Details of the casting process are described elsewhere [7]. For each condition, three identical castings were prepared, one for metallographic observations, and the other two for tensile testing purposes, a total of 48 castings being prepared for the entire investigation. In all cases (metallographic or tensile test sheet specimens), the samples were sectioned from the cast blocks in the horizontal orientation, at varying heights above the water-chilled copper base.

TABLE II Hydrogen measurements ($\text{ml } 100 \text{ g}^{-1}$ Al)

Alloy	AlScan	Leco	ΔH_2 (%)	Remarks
H1				AlScan readings taken <i>after</i> Sr addition to melt
H1T	~ 0.11	~ 0.08	~ 27	
H1S3				
H1TS3				
H2	0.20	0.22	-10	AlScan readings taken <i>after</i> Sr addition to melt
H2T	0.28	0.20	25	
H2S3	0.18	0.38	-109	
H3	0.34	0.325	6.0	AlScan readings taken <i>after</i> Sr addition to melt
H3T	0.306	0.30	2.0	
H3S3	0.24	0.36	-50	
H3TS3	0.23	0.34	-46	
H2S3	0.25	0.22	13	AlScan readings taken <i>before</i> Sr addition to melt
H2TS3	0.244	0.24	1.6	

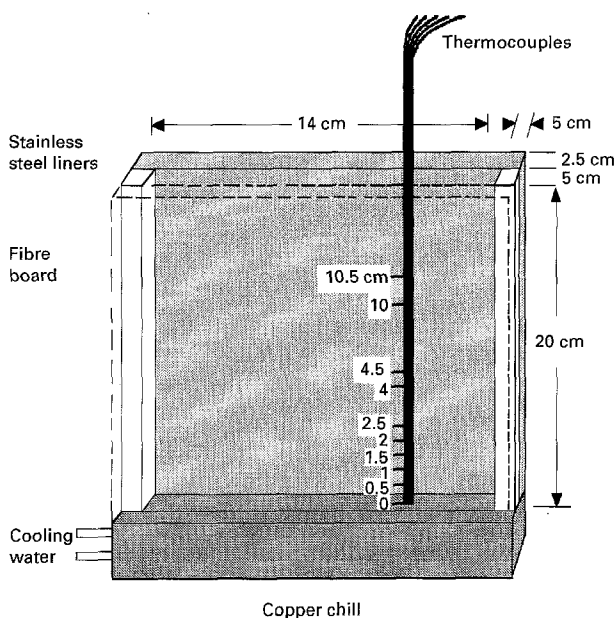


Figure 1 End chill mould [6].

The porosity was quantified using a Leco 2001 image analyser, the measurements being performed on polished sample surfaces ($2 \times 3 \text{ cm}$), cut from the central portion of the casting, at levels of 5, 10, 20, 40 and 100 mm above the endchill bottom. Sheet samples for tensile testing (60 mm long, 20 mm wide and 3 mm thick) were cut at the 5, 20, 40 and 100 mm levels, and heat treated at 180°C for 8 h and then air cooled. Tensile testing was carried out at room temperature using an Instron Universal testing machine at a strain rate of $4 \times 10^{-4} \text{ s}^{-1}$. A strain gauge extensometer (2 in range) was attached to the test specimen for measuring the alloy ductility. The data was analysed using a special software designed for this work. Tensile properties, namely yield stress (YS) at 0.2% offset strain, ultimate tensile strength (UTS), and fracture elongation (EL%) were derived from the data acquisition system.

3. Results and discussion

3.1. Thermal analysis

In order to determine the possible reactions that could take place during solidification under conditions close

to equilibrium ($\sim 0.1\text{--}1^\circ\text{C s}^{-1}$), the liquid metal was poured into a graphite crucible (5.08 cm diameter and 10.16 cm long) that was preheated to 700°C . A thermocouple (K-type) was placed vertically, its tip positioned at 30 mm distance from the bottom of the crucible, and attached to the data acquisition system. Fig. 2 shows the typical temperature–time diagram obtained at a cooling rate of $\sim 0.4^\circ\text{C s}^{-1}$. Three main reactions could easily be separated:

1. Start of solidification $\sim 608^\circ\text{C}$;
2. Formation of Al–Si eutectic $\sim 562^\circ\text{C}$;
3. Precipitation of Al_2Cu phase $\sim 506^\circ\text{C}$.

Fig. 3(a) shows a set of typical cooling curves obtained at the thermocouple positions (positioned horizontally) shown in the endchill mould of Fig. 1. The following observations could be made.

1. The temperature for dendritic onset is the one that is very sensitive to variations in the distance from the chill end. An enlarged portion of Fig. 3(a) showing the drop in the start of solidification temperature is reproduced in Fig. 3(b) and (c), and the results are summarized in Table III.
2. As noted by Tynelius [6] for A356 alloy, the changes in slope that occur in the temperature curve at the onset of eutectic growth and at the solidus temperature are very weak, indicating that the eutectic front grows with an interface that is approximately perpendicular to the growth direction [8].
3. The temperature for the onset of the (Al + Al_2Cu) eutectic reaction cannot be easily distinguished even for the largest distance from the chill end (100 mm). Thus the solidification time is calculated on the basis of the difference between the solidification start temperature and 506°C .

3.2. Porosity Distribution

3.2.1. Radiographic examination

Microfocal radiographs that show the general pore morphology and distribution in as-cast H, HT, HS3 and HTS3 ingots (250 mm long, 130 mm wide and 50 mm thick) are depicted in Figs. 4, 5 and 6 for

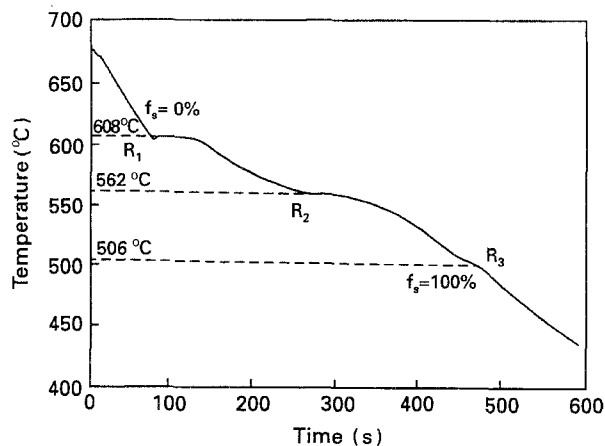


Figure 2 Temperature–time diagram obtained from 319 alloy at a cooling rate $\sim 0.4^\circ\text{C s}^{-1}$. R_1 start of solidification; R_2 formation of Al–Si eutectic; R_3 formation of Al_2Cu , end of solidification.

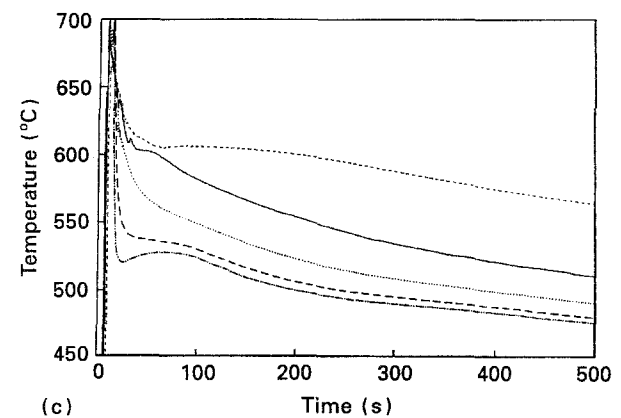
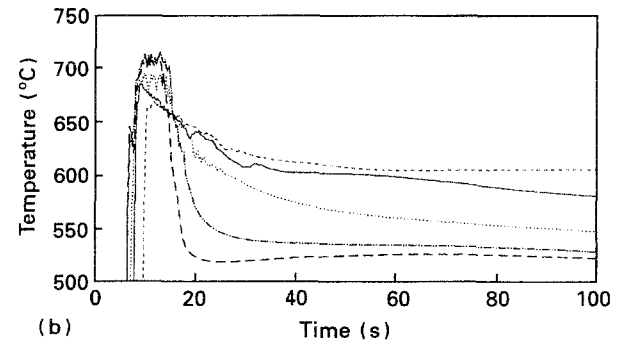
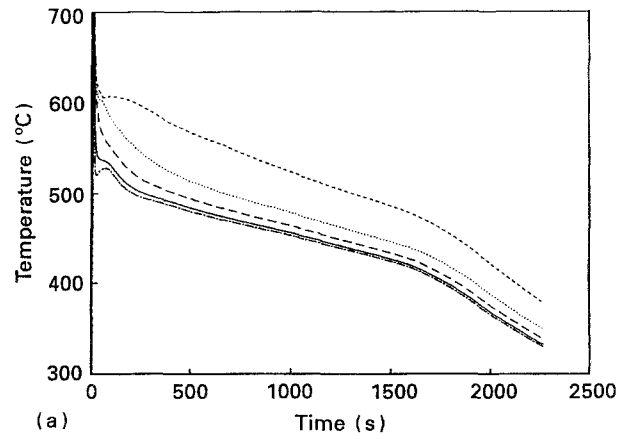


Figure 3 Temperature–time curves recorded in the endchill mould for unmodified, non-grain refined, degassed (H1) alloy: (a) general solidification curves --- no 1; — no 2; - - - no 3; ···· no 4; - - - - no 5; (b) --- no 1; ···· no 2; ···· no 3; — no 4; - - - no 5 and (c) ···· no 1; — no 2; ···· no 3 — no 4; - - - no 5 enlarged portion of the solidification curves: (b) after 100 s; (c) after 500 s.

TABLE III Solidification variants based on thermal analysis data shown in Figs 2 and 3

Mould	Distance from the chill (mm)	Start of solidification temperature (dendritic onset) ($^\circ\text{C}$)	Total solidification time (s)
Graphite	30 mm from crucible bottom	608	490
Endchill	5	520.4	172
	10	537.0	222
	20	561.1	345
	40	601.8	593
	100	607.4	1222

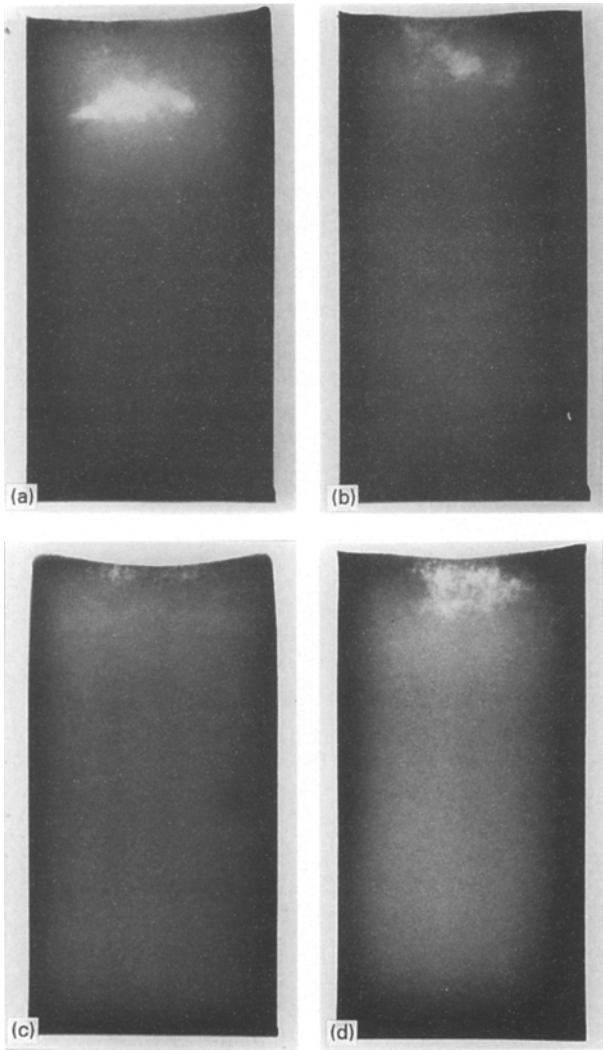


Figure 4 Radiographs obtained from (a) H1; (b) H1T; (c) H1S3; and (d) H1TS3 alloys.

H1, H2 and H3 levels of hydrogen, respectively. The observations gleaned from these radiographs are summarized in Table IV.

In general, for a given hydrogen content, pore density increases with the increase in local solidification time, i.e. proceeding from the bottom to the top of the ingot. Increasing the hydrogen level intensifies the pore density with a marked decrease in the central sump shrinkage cavity. Addition of Sr, as HS3 ingots, contributes significantly to the increase in pore density. Grain refiner addition (measured by 0.02 wt% Ti) decreases the grain size which, in turn, leads to finer pore sizes compared to the H ingots. However, grain refining, in the present case, does not have an influential role in increasing the pore density. In fact, pore densities in HTS3 ingots are somewhat lesser than those observed in HS3 ingots. This observation does not necessarily mean that TiB_2 grain refining particles do not act as nucleation sites for pores [9]. It simply indicates that the original TiB_2 particles in the as-received ingots (measured as ~ 0.073 wt% Ti—Table 1) may have lost their grain refining effect (termed “fading”) during the remelting of the as-received alloy. Thus an additional amount of fresh TiB_2 is needed for effective grain refinement. A similar study was carried out by Tynelius [6] on A356 alloy

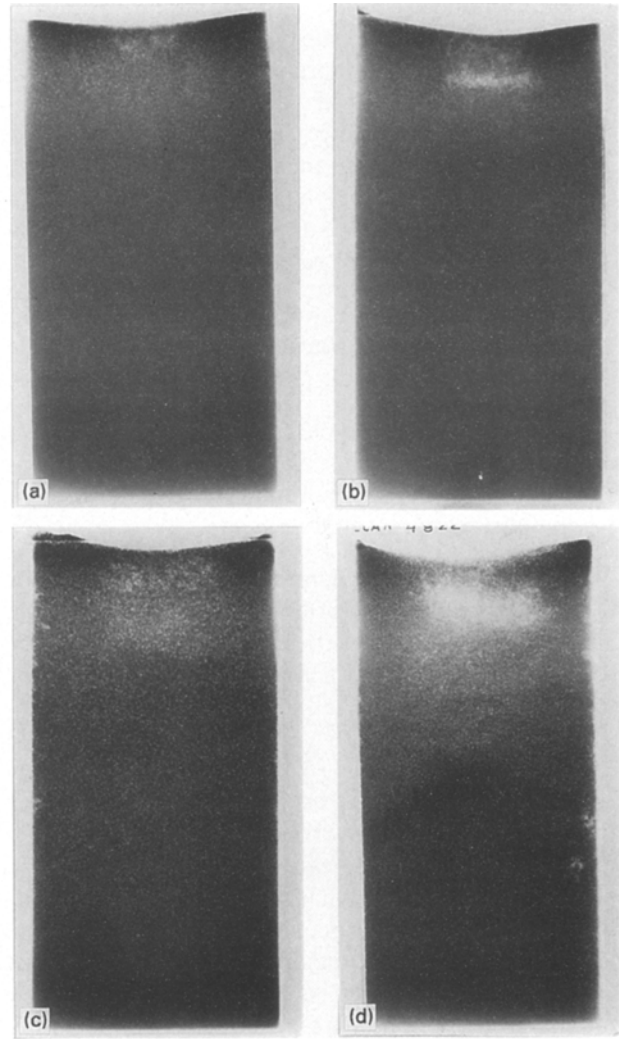


Figure 5 Radiographs obtained from (a) H2; (b) H2T; (c) H2S3; and (d) H2TS3 alloys.

containing 0.04 wt% Ti and 0.001 wt% B. The results showed that grain refiner addition increased pore density through pore nucleation at the TiB_2 particles. The discrepancies between the present findings and those reported in ref. [6] may be related to the effectiveness of the original TiB_2 grain refining particles in the as-received material in the two cases.

3.2.2. Pore morphology

The work of Shivkumar *et al.* [10] on porosity distribution in 319 plate castings shows that the pore morphology is quite irregular even at high hydrogen content, and that the pores are present in both interdendritic and intergranular regions. At small values of local solidification time and low hydrogen contents, the distribution of porosity is skewed towards small pore sizes. When either the hydrogen content or the local solidification time is increased, the pore distribution shifts towards large pore sizes.

Fig. 7(a) represents the microstructure of H1 alloy at 5 mm distance from the chill end. Very small and well scattered pores can be seen (arrowed). At 100 mm distance from the chill, pores are seen in the interdendritic regions. They are disconnected, their lengths approximately the same as the dendrite arms, or even less.

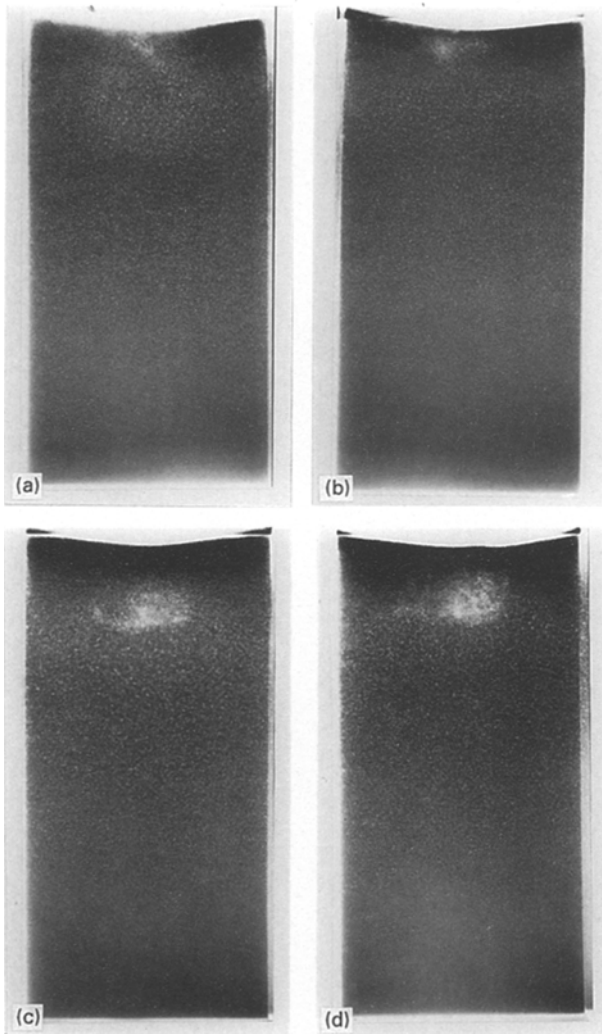


Figure 6 Radiographs obtained from (a) H3; (b) H3T; (c) H3S3; and (d) H3TS3 alloys.

TABLE IV Evaluation of radiographs obtained from alloy castings

Alloy	Evaluation
H1	(a) pronounced sump shrinkage, extending 53 mm from top (b) light mottle (grain) throughout ingot (c) porosity evident 60 mm from chill
H1T	(a) heavy sump shrinkage extending from top 40 mm (b) light mottle, becoming noticeable 80 mm from chill (c) porosity light, becoming evident 115 mm from chill
H1S3	(a) heavy sump shrinkage extending from top 10 mm (b) heavy mottle throughout (c) porosity evident 110 mm from ingot chill, increasing in quantity towards top of ingot
H1TS3	(a) sump shrinkage extends 32 mm to top of ingot (b) moderate mottled appearance starting 20 mm from ingot chill (c) light porosity becoming evident 150 mm from chill
H2	Moderate porosity, moderate grains
H2T	Light to moderate porosity, fine grains
H2S3	Heavy to excessive gas porosity
H2TS3	Heavy gas porosity; pores, however, are of smaller diameter than those observed in H2S3
H3T	(a) ingots are rated from best to worst in quantity and severity of porosity as: H3T, H3, H3S3, H3TS3
H3	
H3S3	(b) a large pocket of sponge shrinkage is noted in the sump of ingots H3S3 and H3TS3
H3TS3	

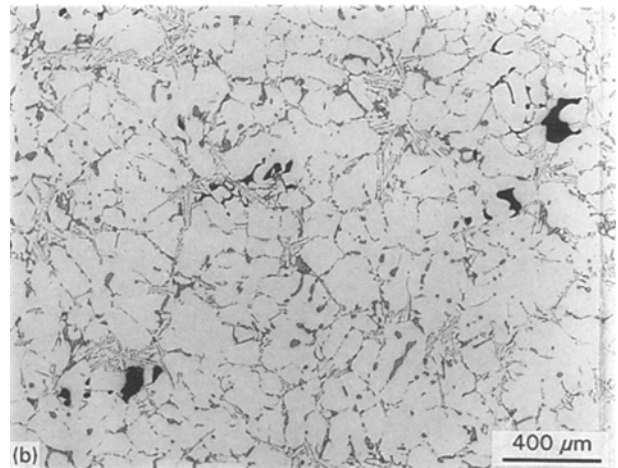
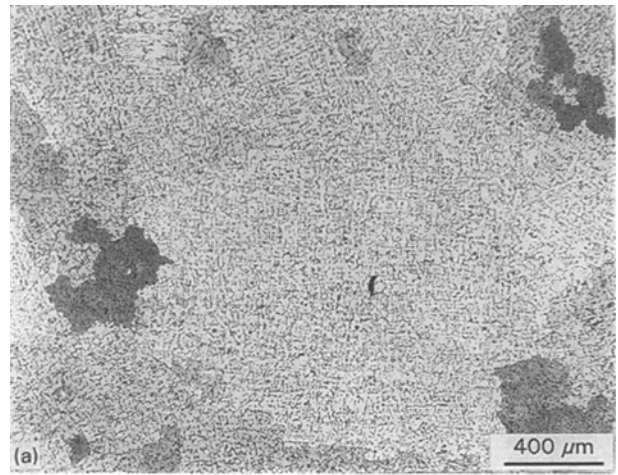


Figure 7 Typical microstructures of unetched samples of H1 alloy taken at (a) 5 mm and (b) 100 mm distance from the chill.

In their parametric study of microporosity in the A356 casting alloy system, Tynelius *et al.* [11] found that in predicting percentage porosity, largest pore size or maximum pore area, the strongest alloy parameter was the Sr content. As an interaction term coupled with hydrogen, it was second only to the solidification time in the intensity of its effect.

Fig. 8(a) shows the microstructure of H1S3 alloy at 5 mm distance from the chill, where not much change in porosity size and distribution is seen above what can be seen in Fig. 7(a). The structure changes dramatically, as the distance from the chill is increased to 100 mm. Figure 8(b) reveals that (a) the pores are rounded and (b) there is an increase in both pore size (as measured by the pore surface area and pore diameter) and porosity volume fraction, which is in good agreement with the findings of Tynelius *et al.* [11].

It is a well established fact that hydrogen is the strongest determinant of all parameters that contribute to porosity formation [12]. This is clearly evident from Fig. 9(a), which represents the microstructure of a specimen taken at 5 mm distance from the chill. Two distinct pore morphologies can be seen, elongated and rounded. At higher solidification time – 100 mm distance from the chill – the majority of pores are rounded (Fig. 9(b)). The hydrogen–strontium (H3S3 alloy) interaction effect on porosity is depicted in Fig. 10(a), where pores are mostly round as opposed

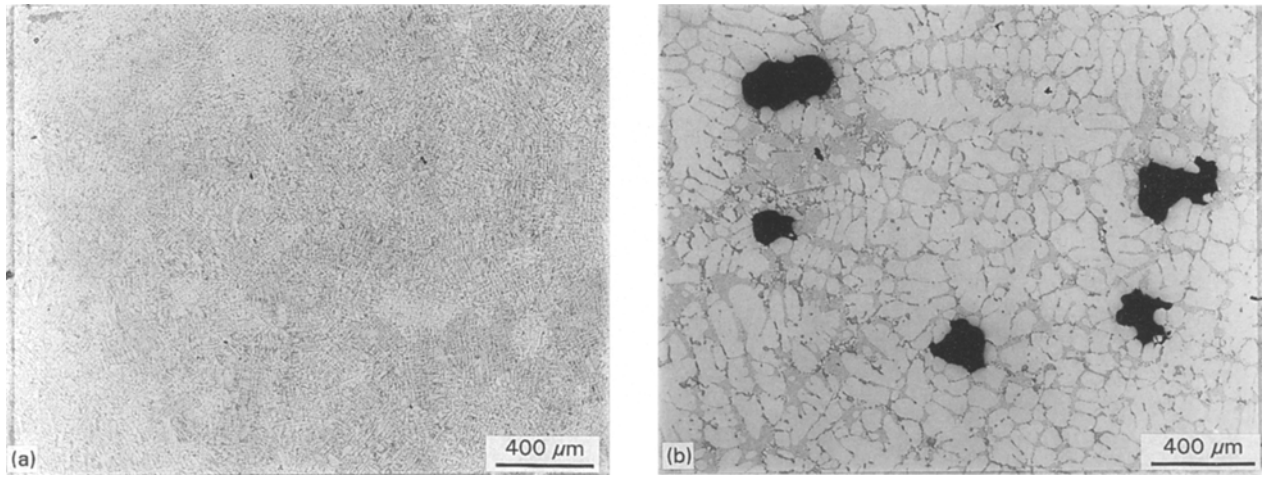


Figure 8 Typical microstructures of unetched samples of H1S3 alloy taken at (a) 5 mm and (b) 100 mm distance from the chill.

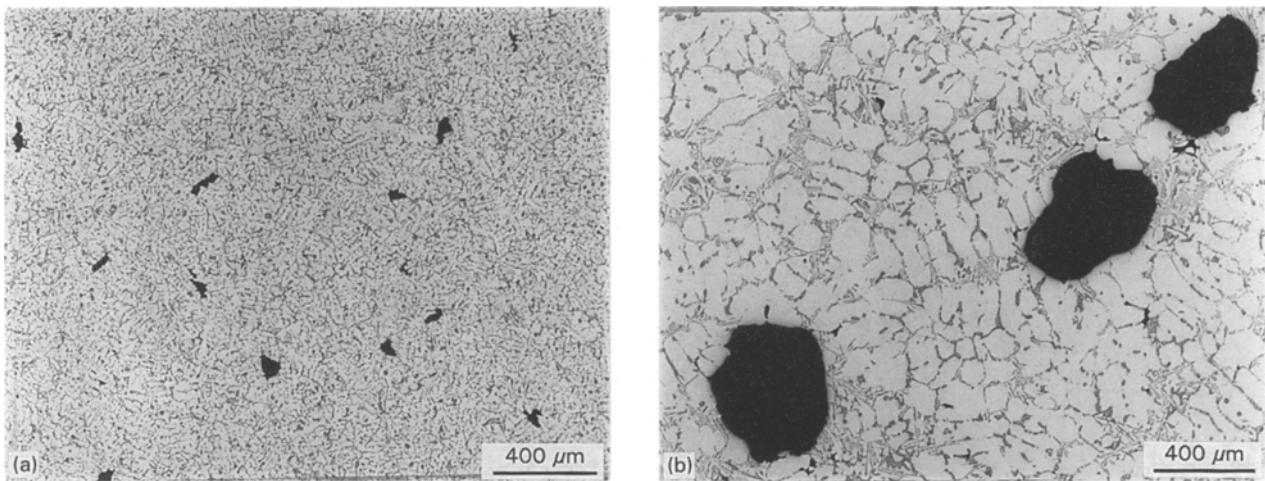


Figure 9 Typical microstructures of unetched samples of H3 alloy taken at (a) 5 mm and (b) 100 mm distance from the chill.

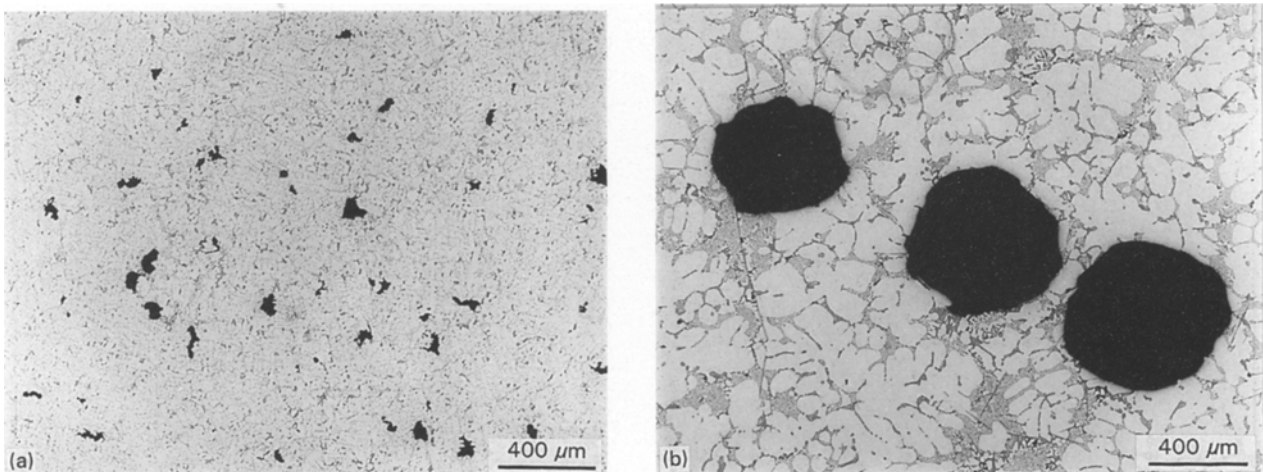


Figure 10 Typical microstructures of unetched samples of H3S3 alloy taken at (a) 5 mm and (b) 100 mm distance from the chill.

to a mixture of rounded and elongated forms shown in Fig. 9(a). This treatment is also associated with an increase in the areal pore density. The effect of increased solidification time is illustrated in Fig. 10(b). Pores are larger and more spherical (round) in this case than those exemplified in Fig. 9(b) for H3 alloy.

In order to study the nucleation mechanism of pores, samples prepared from H3TS3 alloy were etched in Keller's reagent. At low solidification times (i.e. 5 mm distance from the chill) pores (elongated or rounded) were mostly found nucleated at or along the grain boundaries, Fig. 11(a). At intermediate

solidification time (~ 20 mm distance from the chill), while most of the pores were nucleated in the intergranular regions, some were observed in the interdendritic regions (Fig. 11(b) – arrowed). At the highest solidification time (i.e. 100 mm distance from the chill) the possibility of pore nucleation in the intergranular regions was still evident, as shown in Fig. 11(c). These observations are comparable with those reported by Shivkumar *et al.* [10] for 319 alloy.

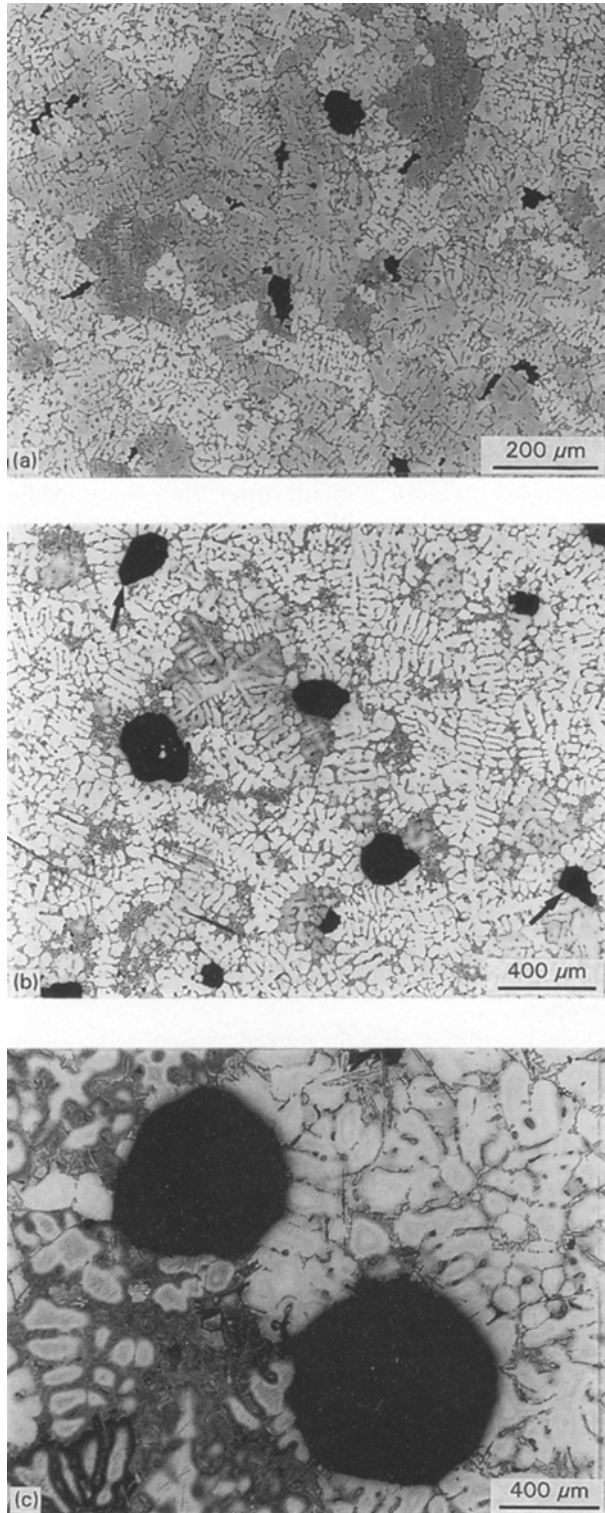


Figure 11 Typical microstructures of etched samples of H3TS3 alloy taken at (a) 5 mm, (b) 20 mm and (c) 100 mm distance from the chill.

3.3. Microstructural Parameters

Variation in dendrite arm spacing (DAS) and grain size as a function of distance from the chill for H1 alloys is shown in Fig. 12. Initially, the DAS increases almost linearly with distance from the chill, at a high rate up to 40 mm. Beyond this distance, the increase in DAS is greatly reduced. Changes in grain size followed a similar trend.

Though the addition of TiB_2 grain refiner does not result in a significant reduction in DAS, its effect on the grain size is remarkable, as depicted in Fig. 12. At high cooling rates grain refined alloy (i.e. H1T) exhibits much finer grain sizes, almost half those measured from H1 alloy. At moderate and low cooling rates, the grain refined alloy grain size is about 70% that of the base H1 alloy. It is worth noting that addition of Sr to H1T alloy (i.e. H1TS3 alloy) negates the refining effect, resulting in grains equal in size to those of the base H1 alloy (circled in Fig. 12). This phenomenon is well illustrated in Fig. 13.

The changes in average Si particle area and length are plotted in Fig. 14. It is clearly evident that the Si particle size is dependent on the α -aluminium dendrite arm spacing. Apparently, for such a low Si content (~ 6 wt%) an addition of 90 p.p.m. Sr is sufficient to promote more or less complete modification of the Si particles, even for cooling rates as low as 0.4°C s^{-1} (DAS ~ 90 μm).

3.4. Tensile Properties

3.4.1. Yield and tensile strengths

As reported earlier [1–3], tensile strength (UTS) is inversely proportional to DAS through linear or parabolic relationships, whereas yield strength (YS) is not a function of DAS.

Fig. 15(a) depicts the variation in UTS and YS for H1 and H1T alloys (hydrogen level ~ 0.1 ml 100 g^{-1} Al) as a function of distance from the chill. The UTS is inversely proportional to DAS (represented by distance from the chill end). The relationships, however, for both alloys are non-linear. It is also noted that at high cooling rates, grain refined H1T alloy is somewhat superior to the non-grain refined H1 alloy. As

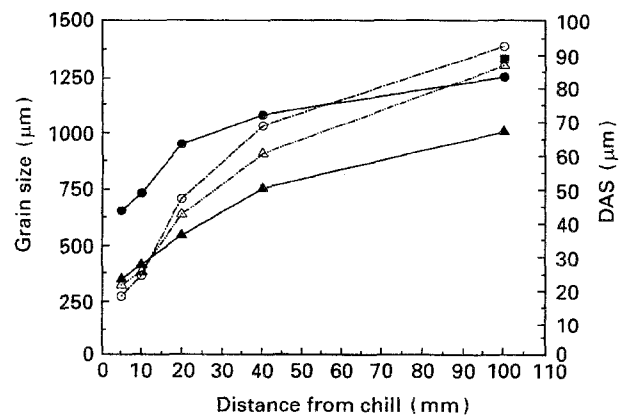


Figure 12 Variation in grain size (● H1; ▲ H1T; ■ H1TS3) and dendrite arm spacing (○ H1; △ H1T) as a function of distance from the chill for H1 and H1T alloys.

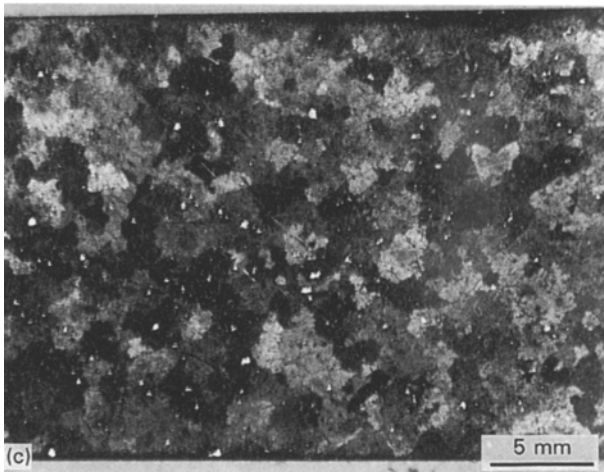
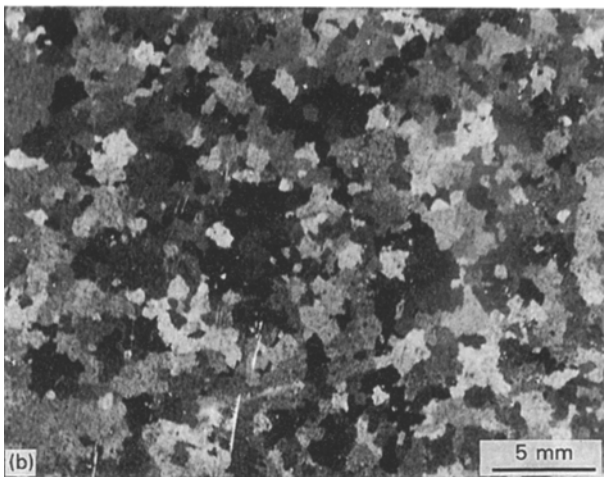
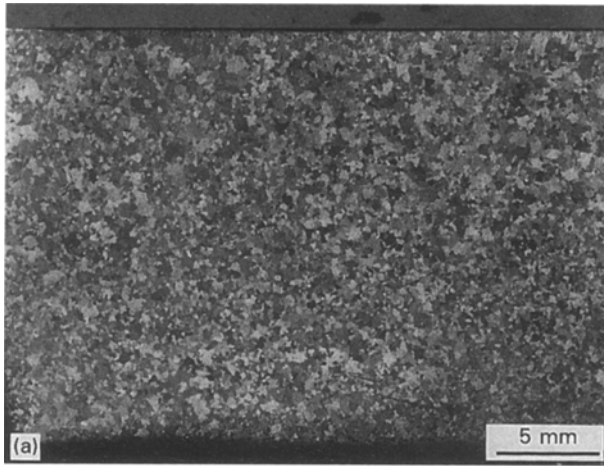


Figure 13 Grain etched samples: (a) H1T alloy, 5 mm; (b) H1T alloy, 100 mm; (c) H1TS3 alloy, 100 mm distance from the chill. Note the pore distribution (white spots) either at the grain boundaries or within the grains.

the cooling rate decreases, the difference in UTS becomes marginal. The values of YS are not affected much by the DAS. The grain refined alloy still offers a better strength compared to the non-grain refined one.

Fig. 15(b) demonstrates the effect of Sr modification on UTS and YS levels with the increase in DAS. It is seen that addition of 300 p.p.m. Sr leads to lower strengths compared to 100 p.p.m. Sr, due to porosity formation as described earlier. It is worth noting here that the YS values for the modified alloys are higher

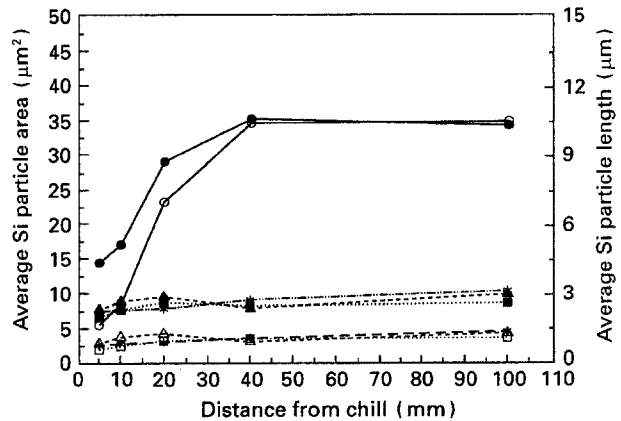


Figure 14 Variation in Si particle average area (○ 10 p.p.m.; △ 90 p.p.m.; □ 180 p.p.m.; -*- 300 p.p.m.) and average length (● 10 p.p.m.; ▲ 90 p.p.m.; ■ 180 p.p.m.; -*- 300 p.p.m.) as a function of distance from the chill for H1, H1S1, H1S2 and H1S3 alloys.

compared to those for the unmodified alloys shown in Fig. 15(a). The general trend exhibited by both UTS and YS, however, is similar to that exhibited by the base H1 alloy.

The yield and tensile strengths obtained from the modified, grain refined castings are displayed in Fig. 15(c). It can be seen that these results, while comparable with those obtained from the grain refined castings (Fig. 15(a)), are still lower than those exhibited by the modified alloy castings (Fig. 15(b)). This observation highlights the effect of Sr in negating the grain refining effect as viewed in Fig. 13.

3.4.2. Percent elongation

The work of Major *et al.* [3] on the mechanical property that correlates best to the microstructure in A356-T61 alloy reveals that the DAS is a measure of the local potential ductility of the alloy casting. Factors such as microporosity or inclusions can reduce the ductility values below the required range. The DAS is a cube function of the solidification time which varies from point to point within the casting; consequently, the ductility level also varies with location.

The ductilities of grain refined as opposed to non-grain refined alloys are shown in Fig. 16(a). As can be seen, the scattering in the data obtained from the non-grain refined alloy is more, compared to the grain-refined one. Unexpectedly, however, the H1T alloy yielded ductilities inferior to those offered by H1 alloy. This result may be attributed to the increase in porosity due to the presence of the TiB₂ grain refining particles in H1T alloy, which provide nucleation sites for the porosity.

It is evident from Fig. 16(b), which relates the variation in ductility with DAS for modified alloys, that modification has a better impact on improving the alloy ductility than grain refining. Paray and Gruzleski [13], however, are of the opinion that porosity caused by modification can negate many of the microstructural benefits by decreasing tensile strength and percentage elongation. When care is taken to prevent gas pick-up, modification with Sr enhances the quality

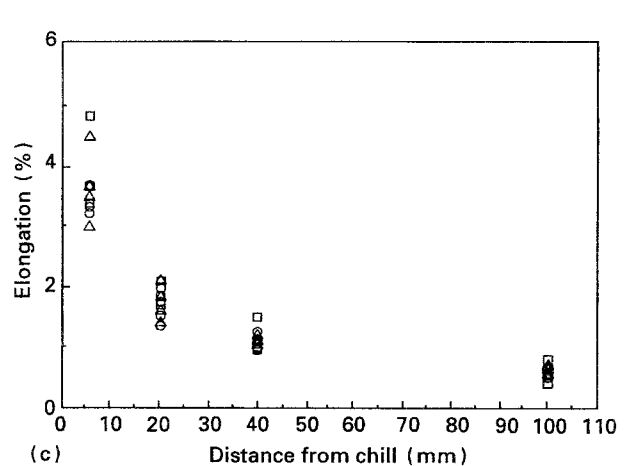
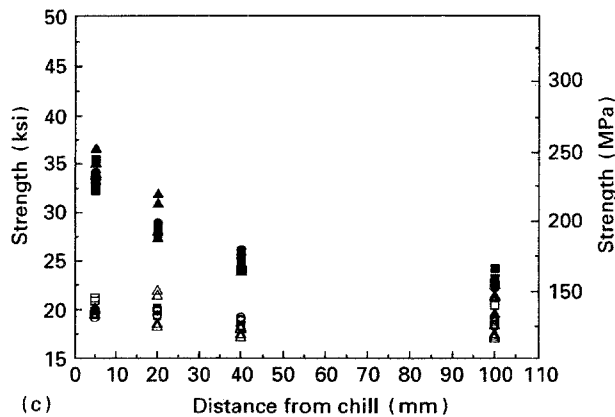
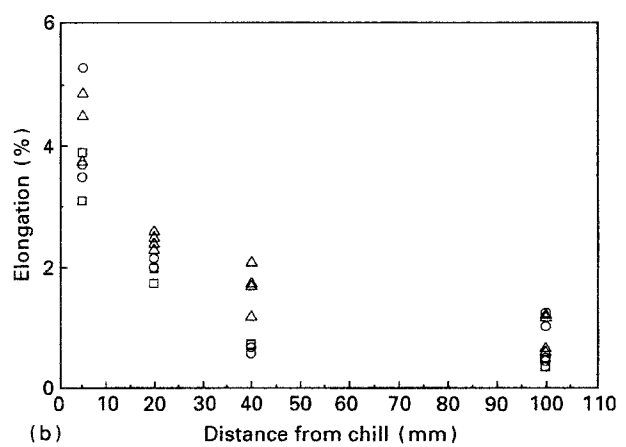
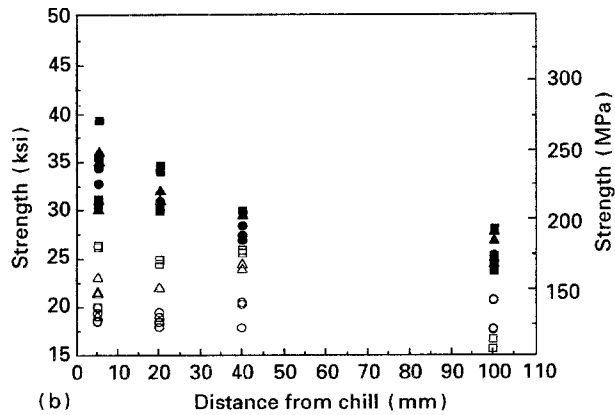
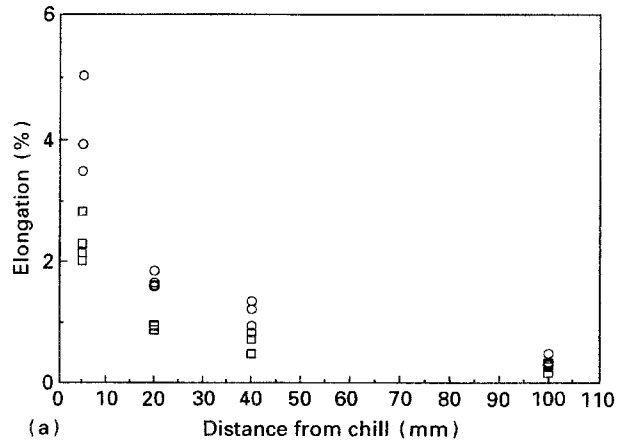
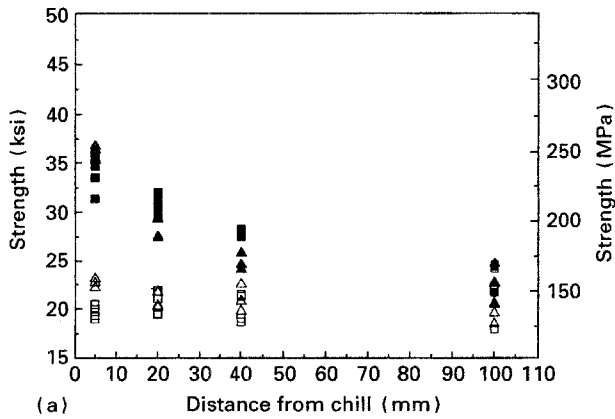


Figure 15 Variation in UTS and YS as a function of distance from the chill: (a) H1 and H1T alloys (■ UTS H1; □ YS H1; ▲ UTS H1T; △ YS H1T); (b) H1S1, H1S2 and H1S3 alloys (■ UTS H1S1; □ YS H1S1; ▲ UTS H1S2; △ YS H1S2; ● H1S3; ○ YS H1S3); (c) H1TS1, H1TS2 and H1TS3 alloys (■ UTS H1TS1; □ YS H1TS1; ▲ UTS H1TS2; △ YS H1TS2; ● UTS H1TS3; ○ YS H1TS3).

Figure 16 Variation in percentage elongation as a function of distance from the chill: (a) H1 (○) and H1T (□) alloys, (b) H1S1 (○), H1S2 (□) and H1S3 (△) alloys, (c) H1TS1 (○), H1TS2 (□) and H1TS3 (△) alloys.

index Q (measured as $Q(\text{MPa}) = \text{UTS}(\text{MPa}) + 150 \log \text{EL}$). Optimum Sr addition for Al-7 wt% Si alloy is around 150 p.p.m. In castings having greater than 300 p.p.m. Sr, a coarse intermetallic phase, Al_4SrSi_2 is observed in the microstructure, that results in a severe drop in Q [14]. The obtained values of Q as a function of distance from the chill in the present work are listed in Table V. It is evident that, except for the highest cooling rate, Sr addition offers a good resistance to degradation in tensile properties.

Small amounts of grain refiner are added to molten aluminium alloys to control the grain structure in

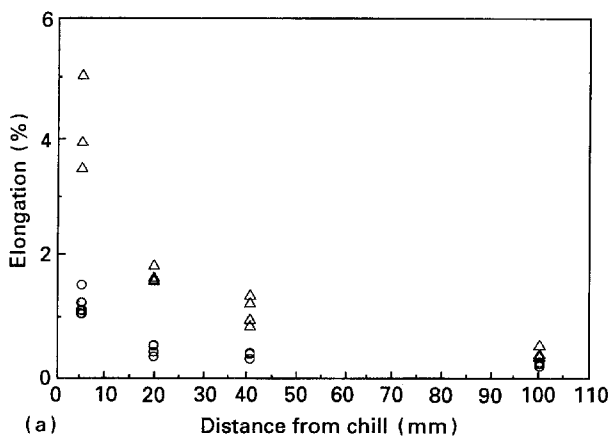
commercial castings. One of the advantages of doing so is the production of a smaller amount and a finer dispersion of porosity in alloys with a long freezing range, such as 319 alloy. Grain refining will also reduce the amount of porosity found in alloys containing moderate to high gas content. The overall effect is to improve the mechanical properties [15].

The combined effect of grain refining and modification on the ductility of 319 castings are demonstrated in Fig. 16(c). The main observation is the consistency of the data as opposed to that shown in Fig. 16(a). In general, the results in Fig. 16(c) are seen to lie in between those for H1 and H1S alloys.

Aluminium alloy melts are characterized by their high affinity for hydrogen absorption during melting and holding [12]. During solidification, the hydrogen

TABLE V Variation in quality index (Q) as a function of distance from the chill

Alloy	Distance from the chill (mm)	Quality index Q (MPa)
H1	5	352.8
	20	262.4
	40	217.0
	100	110.0
H1T	5	362
	20	286
	40	216
	100	187
H1S3	5	333
	20	275
	40	245
	100	187
H1TS3	5	331
	20	248
	40	192
	100	146



is rejected, resulting in the formation of porosity, as described previously, that significantly deteriorates the mechanical properties. An example of the deleterious effect of gas content is shown in Fig. 17(a). Addition of Sr in the presence of hydrogen (H3S3 alloy) increases the amount of porosity even at the highest cooling rate (i.e. 5 mm distance from the chill end, Fig. 10(a)) leading to further drop in ductility, as displayed in Fig. 17(b). Introduction of grain refiner (i.e. H3TS3 alloy) apparently does not cause noticeable changes (Fig. 17(c)). The relationships between the amount of porosity and alloy ductility are summarized in Table VI.

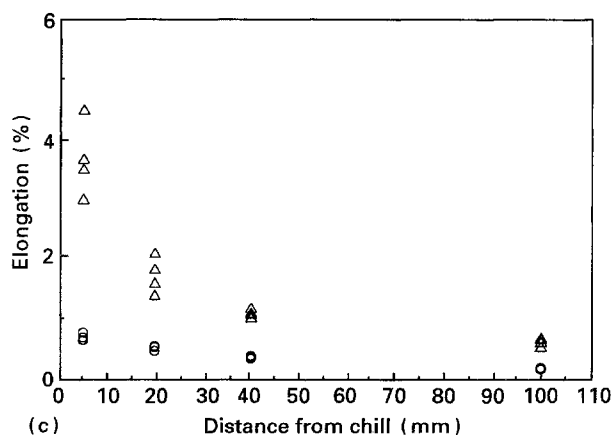
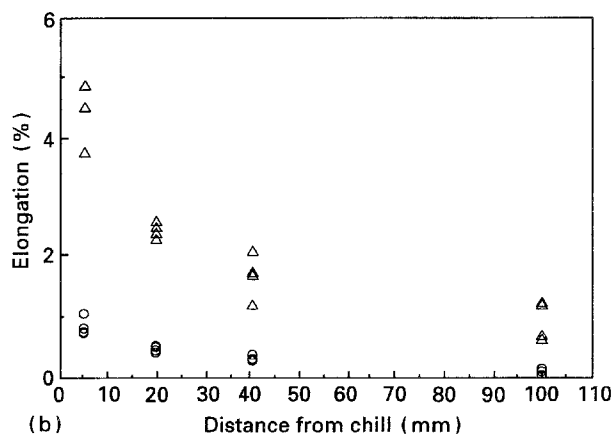


Figure 17 Variation in percentage elongation as a function of distance from the chill: (a) H3 (○) and H1 (△) alloys; (b) H3S3 (○) and H1S3 (△) alloys; (c) H3TS3 (○) and H1TS3 (△) alloys.

TABLE VI Variation in percentage elongation (EL%) as a function of alloy composition, distance from the chill end, and percent porosity

Alloy	Distance from chill (mm)	EL%	Porosity (vol %)	Alloy	Distance from chill (mm)	EL%	Porosity (vol %)
H1	5	4.5 ± 0.5	0.014	H3	5	0.85 ± 0.30	0.513
	20	1.7 ± 0.16	0.024		20	0.5 ± 0.05	1.613
	40	1.1 ± 0.3	0.212		40	0.4	1.795
	100	0.41	0.505		100	0.13	2.495
H1T	5	4.5 ± 0.9	0.029	H3T	5	1.13 ± 0.2	0.582
	20	2.5 ± 1.0	0.115		20	0.55 ± 0.1	1.974
	40	1.1 ± 0.8	0.187		40	0.42 ± 0.05	2.217
	100	0.85 ± 0.5	0.363		100	0.27 ± 0.03	2.694
H1S3	5	3.8 ± 0.6	0.027	H3S3	5	1.25 ± 0.22	0.892
	20	2.5	0.150		20	0.47 ± 0.05	2.638
	40	1.5 ± 0.5	0.696		40	0.34 ± 0.06	2.784
	100	1.0 ± 0.25	1.183		100	0.28	4.830
H1TS3	5	3.7 ± 0.8	0.031	H3TS3	5	0.72 ± 0.08	1.187
	20	1.8 ± 0.3	0.214		20	0.55 ± 0.03	2.970
	40	1.1 ± 0.1	0.347		40	0.4	3.226
	100	0.63 ± 0.2	0.715		100	0.26	3.642

4. Conclusions

A study of the effect of melt treatment, solidification conditions, and porosity on the tensile properties of 319.2 commercial casting aluminium alloy was carried out and the following was found.

1. With respect to solidification time (obtained as a function of DAS) as one parameter, the interaction effect of other parameters, namely hydrogen (H_2), modifier (Sr), and grain refiner (TiB_2) levels, on the porosity follows the order $H_2 > Sr > TiB_2$.
2. At lower solidification times, the pore morphology is mostly elongated, the pores being observed to lie along the grain boundaries. With increasing solidification time, however, the pore morphology tends to be more rounded. Addition of Sr enhances the sphericity of the pores, as well as increases the porosity volume fraction and pore size. TiB_2 tends to disperse the porosity, resulting in smaller pores that are well dispersed over the casting.
3. At low solidification times, pore nucleation takes place predominantly in intergranular regions, while at higher solidification times, the probability of pore nucleation taking place in interdendritic regions is increased.
4. The UTS is very sensitive to variations in the porosity and solidification conditions, and varies in a non-linear fashion with respect to both. The YS is practically unaffected, in accordance with the literature. Ductility is also sensitive to variations in porosity and solidification time, and follows a trend similar to that shown by the UTS.
5. Increasing the porosity volume fraction above 0.5% in the base alloy (unmodified and non-grain refined) reduces the ductility to negligible levels. Sr modification and grain refining allow for increases in the porosity level before the same level of degradation in ductility is observed.

Acknowledgements

The authors would like to thank Mr G. Hayes of Kingston R&D Centre, Alcan International Limited,

Kingston, Ontario for carrying out the radiography tests and analysis. Financial support received from the Natural Sciences and Engineering Research Council of Canada and the Centre québécois de recherche et de développement de l'aluminium (CQRDA) is gratefully acknowledged.

References

1. R. E. SPEAR and G. R. GARDNER, *AFS Trans.* **71** (1963) 209.
2. S. E. FREDERICK and W. A. BAILEY, *Trans. AIME* **242** (1968) 2063.
3. J. F. MAJOR, A. MAKINDE, P. D. LEE, B. CHAMBERLAIN, T. SCAPPATICCI and D. RICHMAN, in International Congress and Exposition on Vehicle Suspension System Advancements, Detroit, Michigan, February 28–March 3, 1994 (SAE International, Warrendale, PA, 1994), p. 117.
4. K. RADHAKRISHNA, S. SESHAN and M. R. SESHADRI, *Trans. Indian Inst. Metals* **34** (1981) 169.
5. E. N. PAN, C. S. LIN and C. R. LOPER, Jr., *AFS Trans.* **98** (1990) 735.
6. K. E. TYNELIUS, Ph.D. Thesis, Drexel University, Philadelphia, 1992.
7. F. T. LEE, J. F. MAJOR and F. H. SAMUEL, *Metall. Mater. Trans. A* **26A** (1994) 1553.
8. "Fundamentals of Solidification", edited by W. KURZ and D. J. FISCHER, Trans. Tech. Publications Ltd., Aedermannsdorf, Switzerland, 3rd Edition, 1989.
9. P. S. MOHANTY, F. H. SAMUEL and J. E. GRUZLESKI, **103** *AFS Trans.* (1995) in press.
10. S. SHIVKUMAR, L. WANG and R. LAVIGNE, in *Light Metals 1993*, edited by S.K. Das (The Minerals, Metals and Materials Society, Warrendale, PA, 1993), pp. 829–838.
11. K. TYNELIUS, J. F. MAJOR and D. APELIAN, *AFS Trans.* **101** (1993) 401.
12. A. M. SAMUEL and F. H. SAMUEL, *J. Mater. Sci.* **27** (1992) 6533.
13. F. PARAY and J. E. GRUZLESKI, *Cast Metals* **5** (1993) 187.
14. B. CLOSSET and J. E. GRUZLESKI, *Metall. Trans. A* **13A** (1982) 945.
15. M. TSUKUDA, T. SUZUKI, I. FUKUI and M. HARADA, *J. Jap. Inst. Metals* **20** (1979) 437.

Received 16 January

and accepted 20 January 1995